ACS Partner Journal

CHEM & BIO ENGINEERING

Open Access

This article is licensed under CC-BY-NC-ND 4.0

pubs.acs.org/ChemBioEng

Article

Computational Insight into Methane–Methanol Coupling and Aromatization over Metal-Modified ZSM-5: From Mechanism to Catalyst Screening

Published as part of Chem & Bio Engineering virtual special issue "Sustainable Catalysis".

Mengnan Sun,[#] Xiaowa Nie,[*,#] Xinwei Zhang, Sirui Liu, Chunshan Song,[*] and Xinwen Guo[*]

Cite This: *Chem Bio Eng.* 2024, 1, 231–244

Read Online

ACCESS | Metrics & More | Article Recommendations | Supporting Information

ABSTRACT: ZSM-5 zeolite modified by molybdenum is one of the promising catalysts for methane dehydroaromatization (MDA). The introduction of methanol to couple with methane over metal-modified ZSM-5 can facilitate the MDA reaction, but the reaction mechanism, optimal energy pathways, and kinetic and selectivity controlling factors remain to be clarified. In this study, periodic density functional theory (DFT) calculations were performed to investigate the mechanism of methane–methanol coupling and aromatization over Mo/ZSM-5. The calculation results showed that the process of methane–methanol coupling to light olefins (mainly ethylene and propylene) was determined by the C–C coupling step, while further aromatization of the ethylene and propylene intermediate was kinetically controlled by the dehydrogenation step involved in the regeneration of the Brønsted acid site over Mo/ZSM-5. The co-adsorption of H_2O produced from methanol dehydration had little effect on methane–methanol coupling to ethylene but increased the rate-limiting barrier for ethylene aromatization to benzene. To further improve the catalytic performance of Mo/ZSM-5, we found that introducing a second metal component such as Co, Ni, or Nb into Mo/ZSM-5 could promote the C–C coupling process and enable these bimetallic combinations to be promising candidates for methane–methanol coupling reactions.

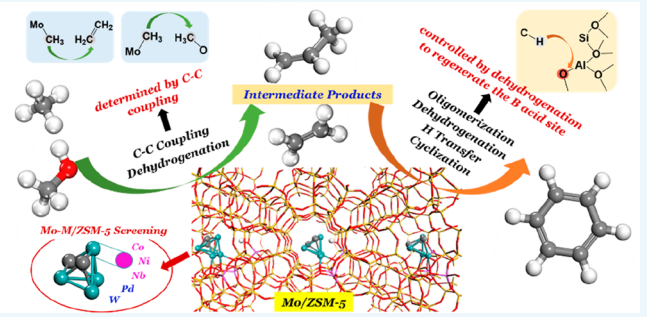

KEYWORDS: *Methane–methanol coupling, Dehydroaromatization, Mo-modified ZSM-5, Reaction mechanism, Density functional theory, Computational screening*

INTRODUCTION

Methane is one of the most stable organic molecules in the world and has abundant global reserves. Selective and directional conversion of methane is a major challenge in the field of catalysis.[1,2] Although the traditional oxidative coupling of methane (OCM) is easy to realize under mild reaction conditions, the methane overoxidation occurring during the process generates a large amount of CO_2, CO, and H_2O, leading to the low utilization of carbon resources. Direct nonoxidative aromatization of methane is a promising process for the simultaneous production of CO_x-free hydrogen and value-added aromatics, which has attracted increasing attention to academia and industry.[3−5] Wang *et al.* used Mo/ZSM-5 as catalyst to conduct the methane dehydroaromatization (MDA) as early as 1993.[6] Afterward, the MDA reaction over metal-modified zeolites has been continually and extensively studied, including studies of the structure and active component of zeolite catalysts, reaction conditions optimization, impact factors of carbon deposition, product selectivity regulation strategy, etc. Among the catalysts studied so far, Mo/ZSM-5 is still widely regarded as one of the best catalysts for MDA. Mo-modified zeolites are recognized as bifunctional catalysts with two different active sites for MDA in the common agreement with experimental studies. The Mo species is the active site for methane activation, while the oligomerization and aromatization of intermediate products mainly occur on the Brønsted (B) acid site of zeolites.[7−10] Wang *et al.* proposed that methane activated over Mo/ZSM-5 generates intermediate products such as ethylene and ethane, which then undergo polymerization, dehydrogenation, and cyclization to yield aromatic hydrocarbons such as benzene and naphthalene.[6] The study of Tan found an enhanced activity and stability of Mo/ZSM-5

Received: September 6, 2023
Revised: November 15, 2023
Accepted: November 30, 2023
Published: January 4, 2024

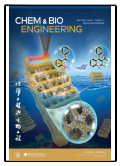

ACS Publications

© 2024 The Authors. Co-published by Zhejiang University and American Chemical Society

https://doi.org/10.1021/cbe.3c00021
Chem Bio Eng. 2024, 1, 231–244

with pretreatment by a mixture of CH_4/Ar/He in catalyzing methane to aromatic hydrocarbons in the absence of an oxidant at 700 °C and revealed that the intermediate product from methane activation was mainly ethylene, which was then transformed into benzene and other aromatics.[11] Although Mo-modified ZSM-5 is a preferable catalyst system for MDA, the coke deposition leading to fast deactivation of catalyst is a major hindrance toward the commercialization of the MDA process. The experimental studies of metal active sites in Mo/ZSM-5 show that the Mo species migrate into the pore of ZSM-5 during the preparation of catalyst and interact with the Brønsted acid site to form the precursor (MoO_x) of active Mo species.[12−17] The MoO_x species adsorbed on ZSM-5 was further reduced to carbidic (MoC_x) and oxycarbidic (MoC_xO_y) by methane during an induction period at the reaction temperature (typically 700 °C).[18−20] The molybdenum carbide (MoC_x) phase with higher catalytic activity than Mo oxide species is the main active species for the conversion of methane into C_2H_x and C_3H_x intermediates.[21−23]

There are still contradictions between the catalytic activity and reaction conditions due to the thermodynamic limitation for MDA. The harsh reaction condition (>700 °C) is favorable for methane conversion but will lead to accelerated catalyst deactivation.[24] The coupling reaction of methane with another co-reactant provides new strategies to solve the aforementioned dilemma of direct methane conversion. Methanol, as a basic organic chemical raw material with mature production technology, can couple with light alkanes to generate value-added products under relatively mild conditions while alleviating the current situation of methanol overcapacity.[25−27] Choudhary *et al.* first explored the simultaneous conversion of methane and methanol into gasoline over Ga-, In-, Zn-, and Mo-modified ZSM-5 catalysts, and they found that the introduction of a small amount of methanol could promote the activation of methane.[28] Their study suggested that the aromatization of methanol mainly occurred at the Brønsted acid site, whereas the process of methane transformation to olefin was catalyzed under the synergistic action of both the metal active site and the Brønsted acid site of metal-modified ZSM-5. Zhang *et al.* found that the addition of a small amount of methanol (CH_4/CH_3OH = 30:1) significantly improved the methane conversion and catalyst stability compared to methane dehydroaromatization in the absence of methanol, with the main products being aromatic hydrocarbons such as benzene, toluene, and xylene over a Mo/ZSM-5 catalyst.[29] Meanwhile, they proposed that carbon from methane mostly reacted to generate aromatic products, whereas carbon from methanol was mainly involved in the alkylation process rather than directly participating in the hydrocarbon pool cycle. Recently, Liu *et al.* reported the methane transformation into light olefins using methanol as a co-reactant over Mo/HZSM-5 at 600 °C and confirmed that the addition of methanol effectively assisted the methane activation.[30] They verified that the C atoms in methane indeed participated in the formation of ethene and benzene products using ^{13}C-labeled methane and GC−MS analysis.

So far, relevant experimental studies on the coupling reaction of methane and methanol over metal-modified zeolites are limited, and the complicated reaction mechanism and the structure−performance relationship of the synergistic catalysis by the metal active site and Brønsted acid site of bifunctional catalysts have not been clearly elucidated yet. Comprehensive theoretical studies on the coupling of methane and methanol for MDA reactions are still lacking, which is detrimental to the development of efficient catalyst systems. Computational studies can identify the key reaction intermediates, transition states, energetically favorable pathways, and key descriptors of the methane−methanol coupling reaction, which are of great significance for understanding the structure-performance relationship and providing a catalyst regulation strategy.

In the present work, density functional theory (DFT) calculations were performed to study the reaction pathways and energy profiles of methane−methanol coupling and aromatization over the Mo/ZSM-5 catalyst. The possible pathways of forming ethylene and propylene intermediates by methane−methanol coupling and the aromatization of these intermediates to aromatic products over Mo/ZSM-5 were comprehensively calculated. The rate-limiting steps for C−C coupling to light olefins and their further aromatization to benzene were identified, and the calculation results show that the benzene formation via the ethylene intermediate is kinetically more favorable than through propylene. The influence of H_2O co-adsorption was further investigated, which was found to have little effect on the ethylene formation but slightly increased the rate-limiting barrier for ethylene aromatization to benzene over Mo/ZSM-5. Then, the rate-limiting C−C coupling step was used as a key descriptor to screen bimetallic Mo-M/ZSM-5 (M = Co, Ni, Pd, Nb, and W) catalyst candidates to improve the catalytic activity for the methane−methanol coupling reaction. The results show that bimetallic Mo−Co/ZSM-5, Mo−Ni/ZSM-5, and Mo−Nb/ZSM-5 further reduce the rate-limiting barrier of C−C coupling to ethylene with Mo−Ni/ZSM-5 as the most promising candidate. This work provides fundamental understanding of reaction pathways and kinetics for the methane dehydroaromatization with methanol as a coreactant and offers useful reference for future catalyst design.

COMPUTATIONAL DETAILS

Computational Models. In this work, one unit cell of the MFI framework with lattice parameters of a = 20.02 Å, b = 19.90 Å, and c = 13.38 Å was used for constructing the periodic structure, which is retrieved from the zeolite database.[31] There are 12 unique tetrahedral T sites (termed T1−T12) per MFI unit cell in the ZSM-5 zeolite. Based on the literature, the Mo carbide species anchored on the Al site is more active than that on the external Si site for the activation of the methane C−H bond.[32] To construct the Mo Lewis acid site, an Al pair was introduced to anchor the active Mo species. The T8-T8 sites within two adjacent five-membered rings of the straight channel were chosen for an Al-pair substitution because the T8-T8 site was found to be more stable to anchor the Mo pieces than other possible substitution sites (e.g. T2-T6, T3-T7, T1-T3, T1-T9, T11-T11) for the Al pair.[32,33] To compensate for the framework negative charge resulting from Al-pair substitution ($2[AlO_4]^-$), two H atoms were introduced and bound to bridge the O atoms of the two −Si−O−Al− units. According to the literature, the Lewis acid site models of the Mo/ZSM-5 catalyst were constructed in the form of $[Mo_4C_2]^{2+}$ by the replacement of H protons with a $[Mo_4C_2]^{2+}$ species since the Mo_4C_2 cluster was found to be more active for methane activation.[5,18,20,33] Meanwhile, a Brønsted acid site was created near the Lewis acid site with a single Al substitution in the intersection of the straight and zigzag channel. For the models of bimetallic Mo-M/ZSM-5, one of

https://doi.org/10.1021/cbe.3c00021
Chem Bio Eng. 2024, 1, 231−244

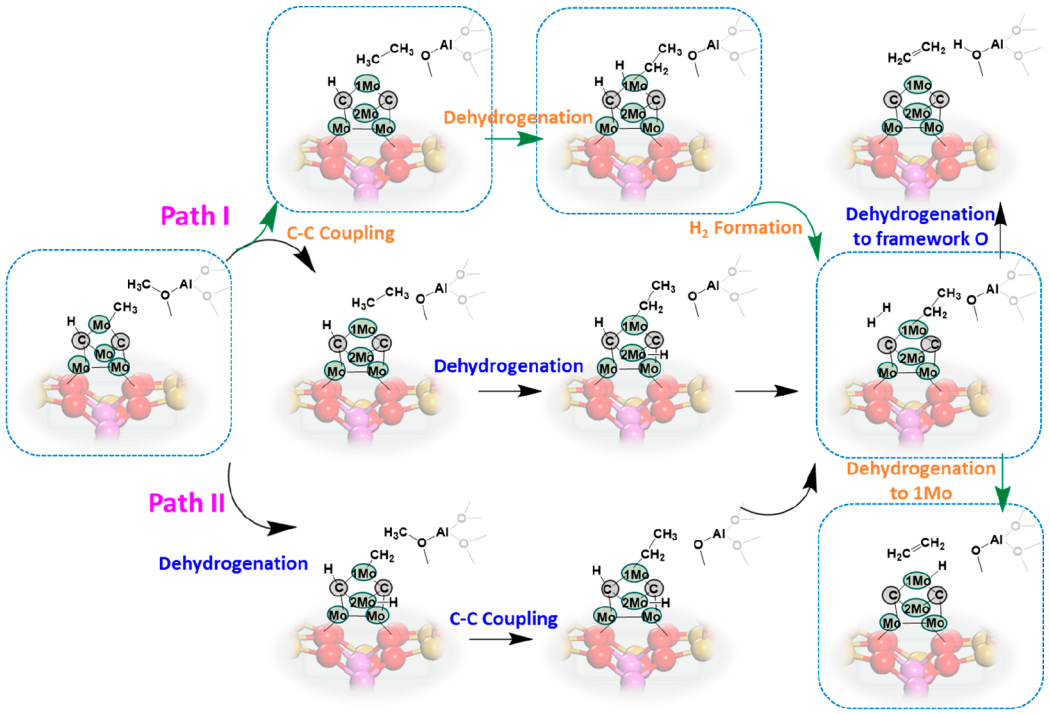

Figure 1. Possible reaction pathways examined for the C−C coupling of Mo−CH_3 with O_{fra}−CH_3 to form ethylene over Mo/ZSM-5.

the Mo atoms that bound to the methyl (CH_3) species was replaced by a second metal M (M = Co, Ni, Pd, Nb, and W). The optimized structures of Mo/ZSM-5 and bimetallic Mo-M/ZSM-5 catalyst models employed in this work are shown in Figure S1.

Computational Methods. All calculations in this work were performed by the periodic density functional theory (DFT) approach as implemented in the Vienna Ab-initio Simulation Package (VASP). The interactions between ion cores and electrons were described by the projector augmented wave (PAW) pseudopotentials, and the electronic structures were calculated using the GGA-PBE method within DFT.[34−37] The electronic states were expended in the plane wave basis with a cutoff energy of 400 eV. The structure convergence criterion was set as the forces on all atoms were less than 0.05 eV/Å while the energy convergence was set to 10^{-5} eV. The PBE+D3 method was adopted to capture the dispersion interactions of zeolite-containing systems.[38,39] All atoms included in the metal/zeolite system together with the adsorbates were fully relaxed and optimized with a Gamma-point of the Brillouin zone restriction. The climbing image nudged elastic band (CI-NEB) method combined with dimer approach were employed to find the transition states, which were confirmed to have only one imaginary frequency along the reaction coordinate according to vibrational frequency calculations.[40] To understand the correlation between the electronic property and catalytic performance, electronic structure calculations were conducted. The Bader charge was calculated to analyze the charge transfer property between the catalyst system and adsorbate. The Crystal Orbital Hamilton Population (COHP) calculations were carried out to analyze the chemical bond interactions in the reaction.

The adsorption energy (E_{ads}) is obtained from the formula $E_{ads} = E_{adsorbate-catalyst} - (E_{catalyst} + E_{adsorbate-gas})$, denoting the energy difference between the total energy of adsorbate with catalyst and the sum of energies of empty catalyst and adsorbate in the gas phase. The reaction energy (ΔE) and activation barrier (E_a) are calculated by the formulas $\Delta E = E_{FS} - E_{IS}$ and $E_a = E_{TS} - E_{IS}$, respectively. Here, E_{IS}, E_{FS}, and E_{TS} represent the DFT calculated electronic energies of the initial state (IS), final state (FS), and transition state (TS), respectively.

RESULTS AND DISCUSSION

1. Reaction Pathways of Methane−Methanol Coupling to Ethylene and Propylene over Mo/ZSM-5. According to previous studies of methane−methanol coupling and MDA reactions in the literature, light olefins (chiefly ethylene and propylene) are observed as the main initial products and important intermediate species, which also exist in final product distribution.[27,29,41] Therefore, understanding the formation mechanism and conversion pathways of ethylene and propylene in the methane−methanol coupling reaction is essential to optimize the reaction conditions, improve the catalyst activity, and tune the product selectivity.

In the first place, the mechanism of methane−methanol coupling to form an ethylene product under the synergistic effect of the Mo metal active site and Brønsted acid site of Mo/ZSM-5 was examined. It is commonly considered that the Lewis acid sites play a dominant role in catalyzing the C−H bond activation of light alkanes over M/ZSM-5, and the Brønsted acid site is the active center for methanol activation.[42−45] Based on this concept, methane adsorption and C−H bond cleavage via dissociation to form the methyl species over the Mo Lewis acid site and methanol adsorption and dehydration over the Brønsted acid site of Mo/ZSM-5 were calculated. The barrier for methane C−H bond cleavage to form the methyl species (Mo−CH_3) is calculated to be 1.15 eV, which is in reasonable agreement with that reported in the literature.[33,46] The adsorption energy of methanol on the Brønsted acid site near the $[Mo_4C_2]^{2+}$ species is calculated to be −1.20 eV, falling in the range of values (−0.96 to −1.34 eV)

https://doi.org/10.1021/cbe.3c00021
Chem Bio Eng. 2024, 1, 231−244

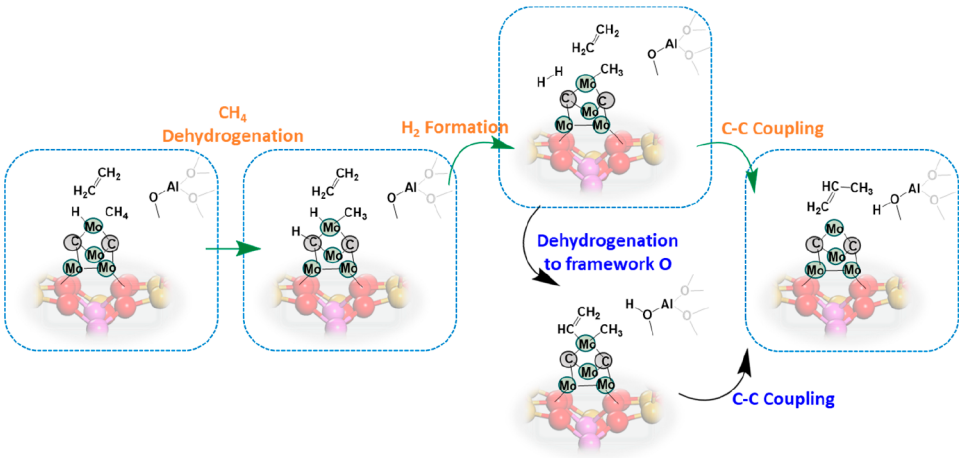

Figure 2. Possible reaction pathways of the C−C coupling of C_2H_4 and CH_4 to form propylene over Mo/ZSM-5.

reported in previous DFT studies over HZSM-5. Methanol adsorption over the $[Mo_4C_2]^{2+}$ metal Lewis site was also investigated (Figure S2), and the calculation result showed that the adsorption energy of methanol on the metal Lewis acid site is −0.76 eV, which is 0.44 eV smaller than that obtained on the Brønsted acid site of Mo/ZSM-5. Therefore, methanol is activated via dehydration by the Brønsted acid site to generate the framework methoxy (O_{fra}−CH_3) and H_2O species with a barrier of 1.25 eV over Mo/ZSM-5. The optimized structures of the initial state, transition state, and final state involved in the activation of methane and methanol are shown in Figure S3.

Subsequently, several possible pathways for C−C coupling of Mo−CH_3 species with O_{fra}−CH_3 to form ethylene were considered, as shown in Figure 1. In Path I, the Mo−CH_3 and O_{fra}−CH_3 species directly go through C−C coupling to form C_2H_6 intermediate first, which then takes off the first H atom to the 1Mo or 2Mo atom of the Mo Lewis acid site to generate the Mo−C_2H_5 intermediate. The first stripped H combines with the H adsorbed on the C atom from methane dissociation to generate an H_2 molecule and desorb. Then, the formed Mo−C_2H_5 intermediate further strips off the second H atom to framework oxygen (O_{fra}) of ZSM-5, regenerating the Brønsted acid site accompanied by the formation of ethylene, or the Mo−C_2H_5 intermediate dehydrogenates to the 1Mo site to generate C_2H_4, as illustrated in Figure 1. In Path II, the Mo−CH_3 species first dehydrogenates to the 2Mo atom of the Mo Lewis acid site, and then the formed Mo−CH_2 intermediate couples with the O_{fra}−CH_3 species to generate Mo−C_2H_5, followed by the two H atoms that bind to the 2Mo atom (2Mo−H) and C atom (C−H, from methane dissociation) generating a H_2 molecule and desorb. The generated Mo−C_2H_5 intermediate continues to dehydrogenate to form ethylene by the same process as in Path I described above.

To identify the minimum energy pathways of methane−methanol coupling to ethylene, we calculated the activation barrier of each elementary step over Mo/ZSM-5. In Path I, the C−C coupling of Mo−CH_3 and O_{fra}−CH_3 to generate the C_2H_6 intermediate has a barrier of 1.40 eV, then the C_2H_6 intermediate dehydrogenation to 1Mo atom forming Mo−C_2H_5 intermediate has a barrier of 0.65 eV, while the C_2H_6 intermediate dehydrogenation to 2Mo atom needs to overcome a large barrier of 1.55 eV. Therefore, the C_2H_6 intermediate dehydrogenation to 1Mo atom is kinetically more favorable. In Path II, the Mo−CH_3 species dehydrogenation to the 2Mo atom to form Mo−CH_2 has a large barrier of 1.95 eV. Then, the formed Mo−CH_2 species coupling with the O_{fra}−CH_3 species to Mo−C_2H_5 intermediate also has to overcome a large barrier of 1.77 eV. Therefore, Path I with C−C coupling of Mo−CH_3 and the O_{fra}−CH_3 as the initial step is kinetically more favorable than Path II with dehydrogenation of the Mo−CH_3 species as the first step.

After the desorption of the formed H_2 molecule, the Mo−C_2H_5 intermediate strips off the second H atom to the framework oxygen (O_{fra}) to regenerate the Brønsted acid site and producing C_2H_4 has a large barrier of 1.80 eV. By contrast, if the Mo−C_2H_5 intermediate takes off the second H atom to the 1Mo atom to generate C_2H_4, the barrier is calculated to be only 0.26 eV, indicating that it is kinetically unfavorable for Mo−C_2H_5 dehydrogenation to regenerate the Brønsted acid site. Based on the above calculation results, the energetically favorable pathway for methane−methanol coupling to ethylene over Mo/ZSM-5 initiates with the M−CH_3 and O_{fra}−CH_3 coupling to generate the C_2H_6 intermediate, followed by the dehydrogenation of the C_2H_6 intermediate to the 1Mo atom to form the Mo−C_2H_5 intermediate. Then the 1Mo−H and C−H combine to form a H_2 molecule and desorb. Finally, the Mo−C_2H_5 intermediate dehydrogenates to the 1Mo atom to generate C_2H_4, which are highlighted by box lines in Figure 1.

Further, the reaction pathways of coupling the intermediate product ethylene with methane to form propylene over Mo/ZSM-5 were calculated, as shown in Figure 2. First, a co-adsorbed methane molecule was introduced into the final structure of the formed ethylene. Methane is activated by dehydrogenation over the Mo Lewis acid site that has already adsorbed a H atom on the Mo site, forming the Mo−CH_3 species, and the dissociated H from methane binds to the C atom of the Mo Lewis acid site. Subsequently, the two H atoms (Mo−H and C−H) combine with each other, generating a H_2 molecule, and desorb. In the next step, two possible situations were considered: in one case, the Mo−CH_3 intermediate from methane dehydrogenation directly couples with ethylene to generate C_3H_6 and regenerate the Brønsted acid site concurrently (concerted path); in the other case, ethylene first dehydrogenates to regenerate the Brønsted acid site and produce the Mo−C_2H_3 intermediate, which then couples with the Mo−CH_3 species to yield C_3H_6 (stepwise path). The activation barrier of each elementary step in the

https://doi.org/10.1021/cbe.3c00021
Chem Bio Eng. 2024, 1, 231−244

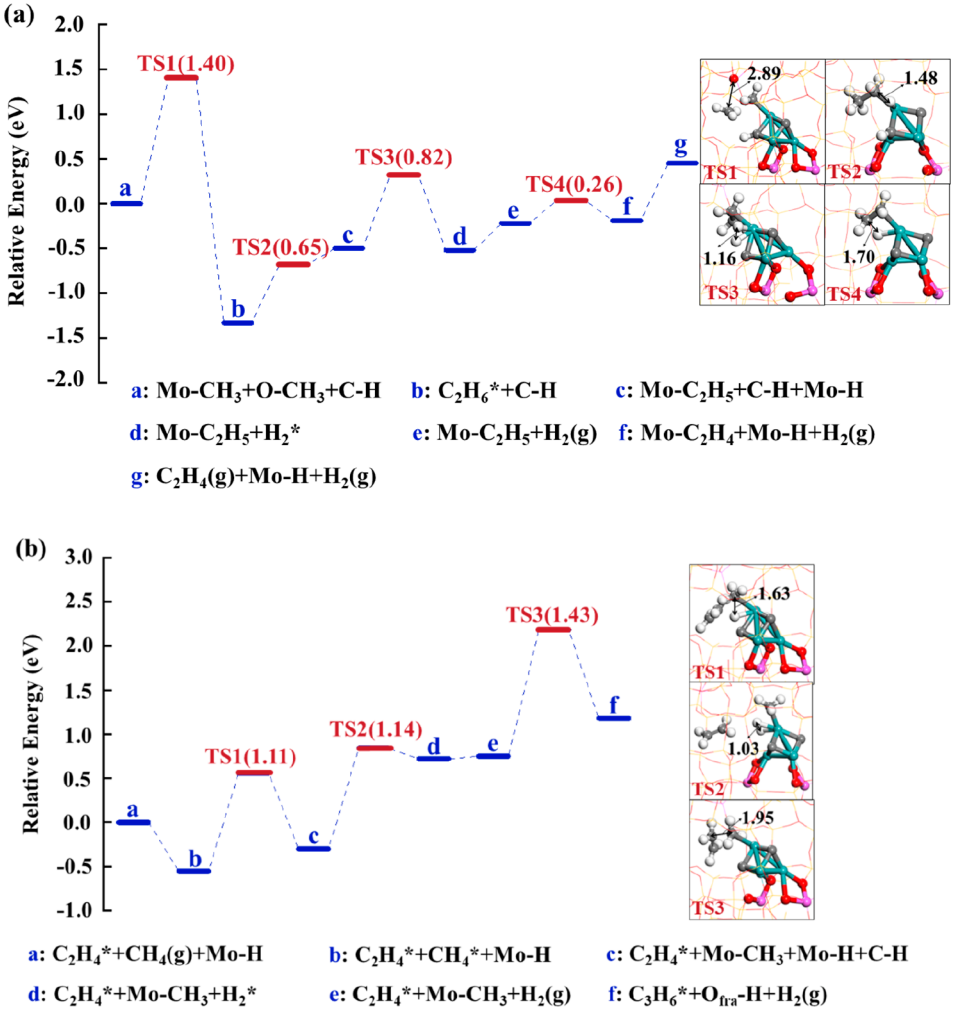

Figure 3. Energy profiles of methane−methanol coupling to form (a) ethylene and (b) propylene over Mo/ZSM-5. (All optimized transition state structures involved are provided in this figure.)

two situations aforementioned was calculated. It shows that the Mo−CH_3 species directly coupling with ethylene to yield propylene has a barrier of 1.43 eV, while the ethylene dehydrogenation to regenerate the Brønsted acid site and the Mo−C_2H_3 intermediate must overcome a barrier larger than 2.50 eV, which is kinetically prohibited. The energetically favorable pathways of coupling the intermediate product ethylene with methane to form propylene over Mo/ZSM-5 are highlighted by box lines in Figure 2 (concerted path). All of the optimized structures of the energetically favorable pathways for C−C coupling to ethylene and propylene are provided in Figure S4.

2. Catalytic Performance of Methane−Methanol Coupling to Ethylene and Propylene over Mo/ZSM-5. Based on the calculation results above, the C−C coupling reactions to form ethylene and propylene proceed slowly due to higher rate-limiting barriers (1.40 and 1.43 eV) compared to the barriers for methane activation via C−H bond dissociation (1.15 eV) and methanol activation via dehydration (1.25 eV). Thus, we focus on the C−C coupling processes over the Mo/ZSM-5 catalyst. The energy diagrams associated with the energetically favorable pathways of C−C coupling to ethylene and propylene together with all transition state structures involved are provided in Figure 3. As shown in Figure 3(a), C−C coupling of the Mo−CH_3 species from methane dissociation and the O_{fra}−CH_3 species from methanol dehydration to form C_2H_6 intermediate has a barrier of 1.40 eV, which is followed by the C_2H_6 intermediate dehydrogenation to generate the Mo−H and Mo−C_2H_5 intermediate with a barrier of 0.65 eV. Subsequently, the two H atoms (Mo−H and C−H) combine to generate a H_2 molecule that needs to overcome a barrier of 0.82 eV. The desorption energy of H_2 is calculated to be 0.30 eV. Finally, the Mo−C_2H_5 intermediate further dehydrogenates to Mo atom to generate C_2H_4 with a small barrier of only 0.26 eV. C_2H_4 desorption from the Mo Lewis acid site has an energy of 0.64 eV, leaving a H atom (Mo−H) on the Mo Lewis acid site. The rate-limiting step of C−C coupling to ethylene over Mo/ZSM-5 is the Mo−CH_3 and O_{fra}−CH_3 coupling to form the C_2H_6 intermediate with a barrier of 1.40 eV.

As shown in Figure 3(b), the intermediate product ethylene and methane co-adsorb on the Mo Lewis acid site with an H atom (Mo−H) in the initial state structure. The second methane activation to form the Mo−CH_3 species over the Mo Lewis acid site with an absorbed H needs to overcome a barrier of 1.11 eV, which is almost the same as that of the first methane activation (1.15 eV), indicating that there is little effect of adsorbed H on methane C−H bond activation over the Mo Lewis acid site. Then, the generated C−H from the second methane activation combines with Mo−H to form a H_2

https://doi.org/10.1021/cbe.3c00021
Chem Bio Eng. 2024, 1, 231−244

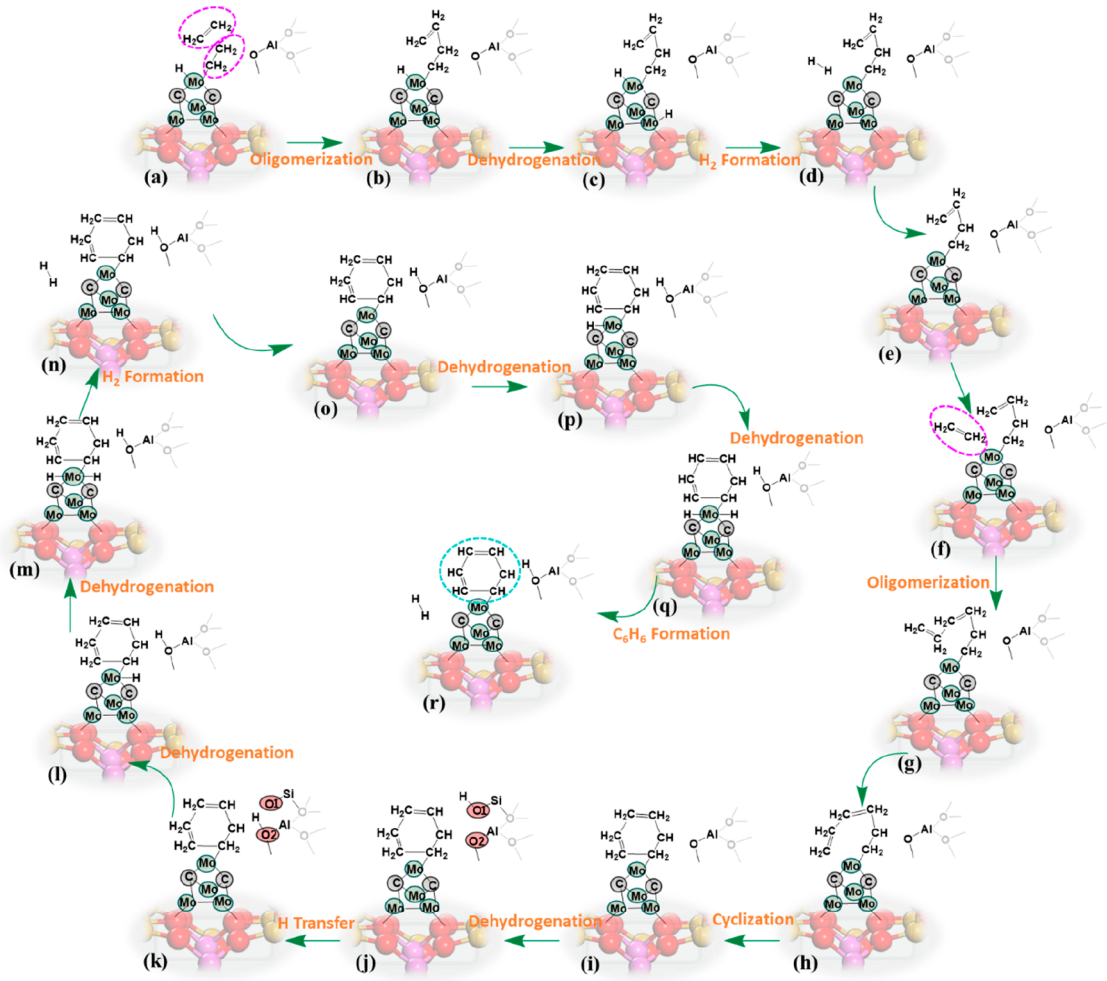

Figure 4. Reaction pathways of ethylene aromatization to benzene over Mo/ZSM-5.

molecule with a barrier of 1.14 eV. The desorption energy of H_2 from the Mo Lewis acid site is calculated to be 0.03 eV. Finally, the Mo−CH_3 intermediate directly couples with C_2H_4 to generate C_3H_6 and concurrently regenerate the Brønsted acid site with a barrier of 1.43 eV, which is the rate-limiting step of propylene formation from C−C coupling of ethylene and methane over Mo/ZSM-5.

Comparing the energy pathways of methane−methanol coupling to form ethylene and propylene over Mo/ZSM-5, we found that the rate-limiting steps of ethylene and propylene formation are both involved in the processes of C−C coupling, indicating that the C−C coupling barrier is a key energy descriptor to dictate the catalytic performance of Mo/ZSM-5 toward methane−methanol coupling to produce light olefins. In addition, the rate-limiting barriers of ethylene and propylene formation by methane−methanol coupling over Mo/ZSM-5 are very close (1.40 *vs* 1.43 eV), indicating that the formation of these intermediate products is competitive over Mo/ZSM-5.

3. Ethylene Aromatization Mechanism over Mo/ZSM-5. The light olefin intermediate products go through a series of reactions involving polymerization, dehydrogenation, and cyclization to form aromatic hydrocarbons eventually in methane−methanol coupling and MDA reactions over metal/zeolites. Therefore, we continued to explore the mechanism and reactivity for the aromatization of the intermediate products ethylene and propylene over Mo/ZSM-5. Benzene was used as the representative aromatic product since it dominated the final aromatic products as evidenced in relevant experimental studies.[47,48]

As shown in Figure 4, the aromatization of ethylene over Mo/ZSM-5 typically goes through sequential steps involving oligomerization, dehydrogenation, cyclization, and further dehydrogenation to aromatic products. The energy diagrams of aromatization of ethylene to benzene are provided in Figure 5 with all transition state structures included. In the initial step, another ethylene molecule was introduced into the final structure of the formed ethylene and co-adsorbed with it over the active site of Mo/ZSM-5 (state a in Figure 5(a)). Then, these two species go through the oligomerization reaction to generate the C_4 hydrocarbon species (Mo−C_4H_8, intermediate b in Figure 5(a)) with a barrier of 0.62 eV. In the next scenario, two different processes of dehydrogenation of the Mo−C_4H_8 intermediate to Mo Lewis acid site were investigated. One case is the Mo−C_4H_8 intermediate dehydrogenation to the C atom of the Mo Lewis acid site with a barrier of 0.56 eV, but the subsequent step of C−H and Mo−H combination to form a H_2 molecule is very difficult to occur due to a high barrier of more than 2.00 eV. In the other case, the Mo−C_4H_8 intermediate dehydrogenates to the Mo atom of the Mo Lewis acid site with a barrier of 1.13 eV, and the reaction energy of the subsequent H_2 generation step is endothermic at 0.40 eV without a barrier. Therefore, the

https://doi.org/10.1021/cbe.3c00021
Chem Bio Eng. 2024, 1, 231−244

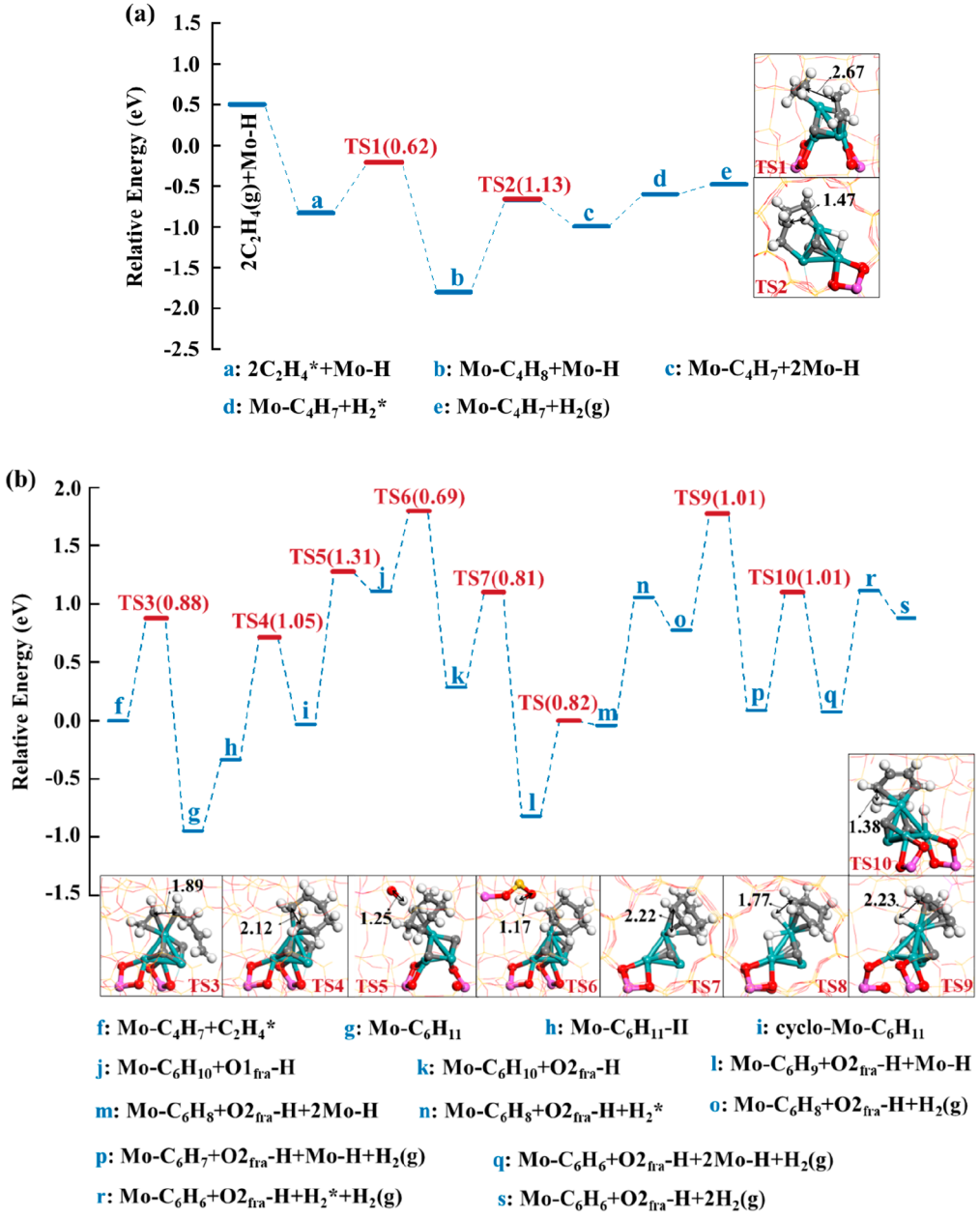

Figure 5. Energy profiles of ethylene aromatization to benzene over Mo/ZSM-5, (a) the process of first two ethylene coupling to Mo−C_4H_7 and (b) the process of introducing the third ethylene to generate benzene. (All optimized transition state structures involved are provided in this figure.)

energetically favorable pathway is the Mo−C_4H_8 intermediate dehydrogenation to the Mo atom to form Mo−C_4H_7 (intermediate c in Figure 5(a)), and the subsequent dehydrogenation is thus considered to occur on the Mo atom of the Mo Lewis acid site. After the two Mo−H species generating H_2 (intermediate d in Figure 5(a)) and H_2 desorption (state e in Figure 5(a)) (with a reaction energy of 0.40 eV and desorption energy of 0.12 eV, respectively), the third ethylene molecule was introduced to co-adsorb with Mo−C_4H_7 over the active site (intermediate f in Figure 5(b)). Then, the Mo−C_4H_7 intermediate and ethylene oligomerize to form a chain-structured C_6 hydrocarbon intermediate (Mo−C_6H_{11}, intermediate g in Figure 5(b)), with a barrier of 0.88 eV. In the next step, the chain-structured Mo−C_6H_{11} intermediate goes through a structural change intended to form an almost annular transitional structure (Mo−C_6H_{11}-II, intermediate h in Figure 5(b)) with a reaction energy of 0.61 eV, followed by the cyclization of Mo−C_6H_{11}-II to form the ring-structured cyclo-Mo−C_6H_{11} with a barrier of 1.05 eV (intermediate i in Figure 5(b)). It is difficult for cyclo-Mo−C_6H_{11} intermediates to direct dehydrogenation to the framework O connected to Al to regenerate the Brønsted acid site (barrier of 2.3 eV), due to the spatial confinement effect of zeolite pores. Therefore, it is considered that the cyclo-Mo−C_6H_{11} intermediate first dehydrogenates to the framework O connected to Si adjacent to the Al site (O1 marked in Figure 4), forming a transition intermediate structure with a barrier of 1.31 eV (Mo−C_6H_{10} + $O1_{fra}$−H, state j in Figure 5(b)), followed by the H transfer to framework O connected to Al (O2 marked in Figure 4) to regenerate the Brønsted acid site and simultaneously produce the Mo−C_6H_{10} intermediate (intermediate k in Figure 5(b)), which needs to

https://doi.org/10.1021/cbe.3c00021
Chem Bio Eng. 2024, 1, 231−244

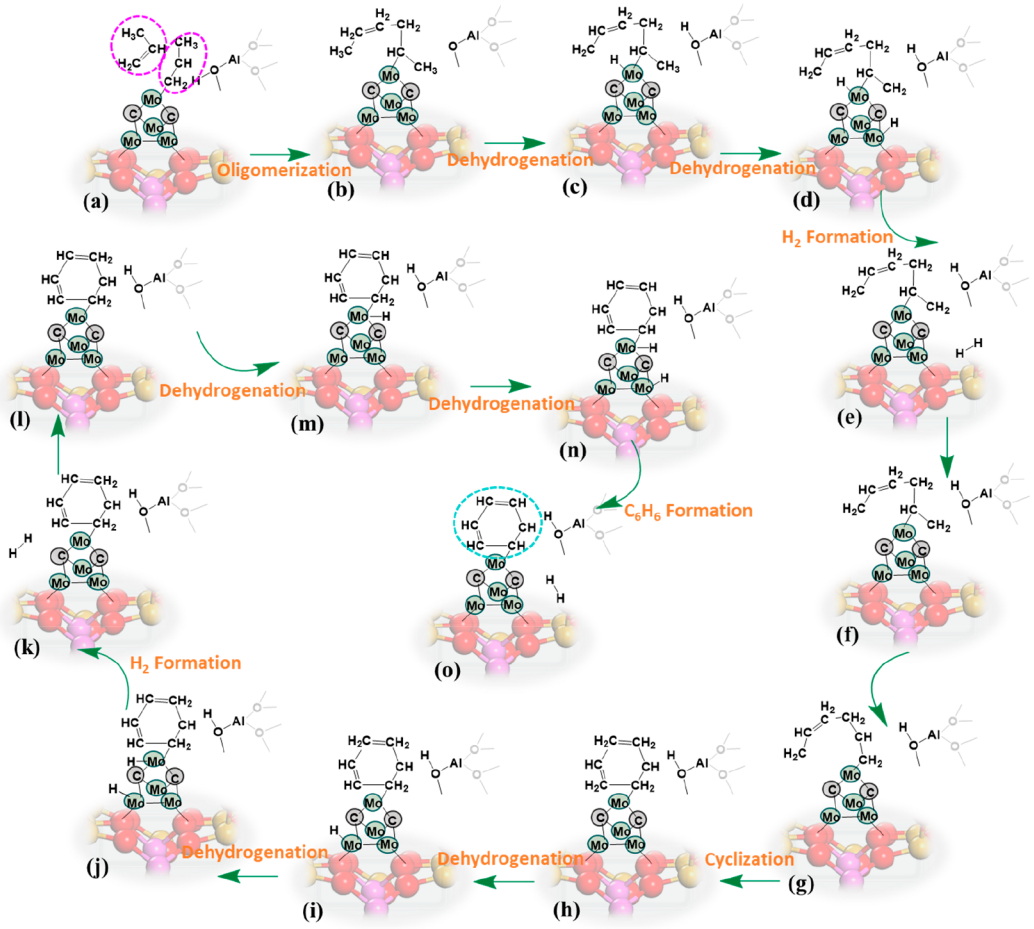

Figure 6. Reaction pathways of propylene aromatization to benzene over Mo/ZSM-5.

overcome a barrier of 0.69 eV. The cyclic Mo−C_6H_{10} intermediate sequentially takes off two H atoms to the Mo site to form the Mo−C_6H_8 species with barriers of 0.81 and 0.82 eV, respectively (intermediates l and m in Figure 5(b)). The generation of H_2 from the two Mo−H species (intermediate n in Figure 5(b)) needs to overcome a reaction energy of 1.10 eV, and H_2 desorption is an exothermic process by releasing an energy of 0.28 eV. Then, the cyclic Mo−C_6H_8 intermediate (state o in Figure 5(b)) undergoes two sequential dehydrogenation steps to generate benzene. The barriers of cyclic Mo−C_6H_8 dehydrogenation to form cyclic Mo−C_6H_7 and benzene formation from cyclic Mo−C_6H_7 dehydrogenation (intermediate p and q in Figure 5(b)) are both 1.01 eV. The reaction energy for the last two Mo−H species forming the H_2 molecule is 1.04 eV (intermediate r in Figure 5(b)), and the desorption of H_2 (state s in Figure 5(b)) is also an exothermic process with a reaction energy of −0.23 eV. The optimized structures of all states involved in ethylene aromatization to benzene over Mo/ZSM-5 are provided in Figure S5. As demonstrated in Figure 5(a) and (b), the rate-limiting step for the aromatization reaction is the first dehydrogenation involved in regeneration of the Brønsted acid site; i.e., the cyclo-Mo−C_6H_{11} intermediate dehydrogenates to framework oxygen O1, with a barrier of 1.31 eV. Unlike methane and methanol coupling to form ethylene and propylene over Mo/ZSM-5, which is mainly controlled by the C−C coupling reaction (rate-limiting barriers of 1.40 and 1.43 eV, respectively), the barriers of C−C oligomerization steps in the ethylene aromatization process are not high (0.62 and 0.88 eV). The DFT results reveal that the process of Brønsted acid site regeneration through hydrocarbon intermediate dehydrogenation is a key aspect affecting the ethylene aromatization performance over Mo/ZSM-5.

4. Propylene Aromatization Mechanism over Mo/ZSM-5. Based on the proposed mechanism, an optimal reaction route for intermediate product propylene aromatization to benzene over Mo/ZSM-5 is illustrated in Figure 6. The energy diagram and all optimized transition state structures involved in this process are listed in Figure 7. In the initial step, two propene molecules are coadsorbed (state a in Figure 7) and oligomerized with each other under the synergistic effect of the Brønsted acid site and Mo Lewis acid site to generate the chain-structured C_6 hydrocarbon ((Mo−C_6H_{13}, intermediate b in Figure 7). The propene oligomerization is a spontaneous process with a reaction energy of −0.57 eV, showing that the Brønsted acid site facilitates the oligomerization reaction greatly. The chain-structured Mo−C_6H_{13} intermediate further dehydrogenates to framework O to regenerate the Brønsted acid site, while taking off another H atom to the Mo site and forming Mo−C_6H_{11} species (intermediate c in Figure 7). This step has to overcome a barrier of 1.56 eV. The Mo−C_6H_{10} intermediate (intermediate d in Figure 7) is formed by the dehydrogenation of Mo−C_6H_{11} to the Mo site, which has a barrier of 1.45 eV. The formation of a H_2 molecule by two Mo−H species (state e in Figure 7) is almost a thermodynamic equilibrium step (reaction energy

https://doi.org/10.1021/cbe.3c00021
Chem Bio Eng. 2024, 1, 231−244

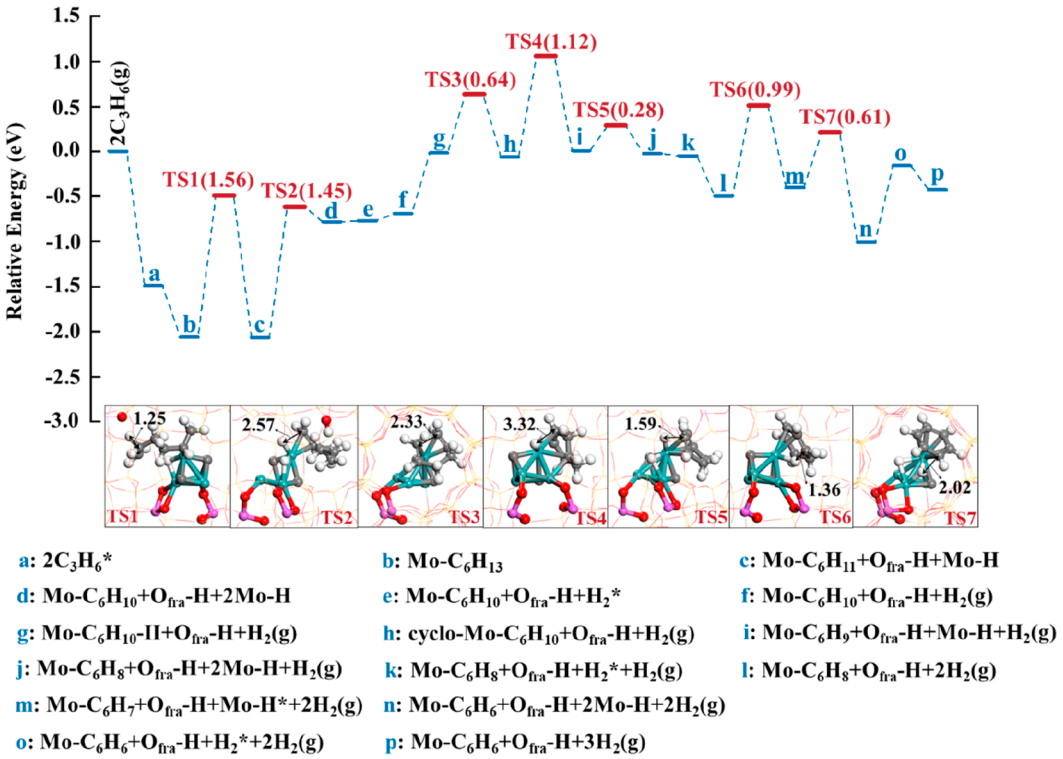

Figure 7. Energy profiles of the aromatization of propylene to benzene over Mo/ZSM-5. (All optimized transition state structures involved are provided in this figure.)

0.01 eV) without a barrier, and the desorption of the H_2 molecule from the active site only has an energy of 0.08 eV (state f in Figure 7). In another process we considered, the chain-structured Mo−C_6H_{13} intermediate takes off two H atoms sequentially to the C atom and Mo atom of the Mo Lewis acid, but the barrier of C−H and Mo−H combination to form H_2 molecule is very high (more than 2.00 eV) and thus is excluded. The formed chain-structured Mo−C_6H_{10} intermediate undergoes a structure deformation intended to form a ring-like configuration (Mo−C_6H_{10}-II, intermediate g in Figure 7), and this step is an endothermic process with a reaction energy of 0.67 eV. The transitional intermediate structure Mo−C_6H_{10}-II further goes through a cyclization reaction to form the ring-structured cyclo-Mo−C_6H_{10} intermediate (intermediate h in Figure 7), which requires a barrier of 0.64 eV. The cyclo-Mo−C_6H_{10} dehydrogenation to the Mo atom to form Mo−C_6H_9 (intermediate i in Figure 7) needs to surmount a barrier of 1.12 eV, followed by continuous dehydrogenation of Mo−C_6H_9 to another Mo atom to form the Mo−C_6H_8 intermediate (intermediate j in Figure 7) with a small barrier of 0.28 eV. The combination of two Mo−H species to form a H_2 molecule (state k in Figure 7) is almost a thermodynamic equilibration process (reaction energy of −0.03 eV), followed by the desorption of H_2 from the active site, which is exothermic by −0.45 eV (state l in Figure 7). The Mo−C_6H_8 intermediate continuously takes off two H atoms to generate benzene eventually, with dehydrogenation barriers of 0.99 and 0.61 eV, respectively (intermediate m and n in Figure 7). The combination of two Mo−H species has a reaction energy of 0.85 eV to generate another H_2 molecule (state o in Figure 7), and then releasing the H_2 molecule to the gas phase is exothermic by −0.27 eV (state p in Figure 7). The optimized structures of all states involved in propylene aromatization over Mo/ZSM-5 are provided in Figure S6.

It is noted that the rate-limiting step of propylene aromatization to benzene over Mo/ZSM-5 is the dehydrogenation of the chain-structured C_6 hydrocarbon intermediate to regenerate the Brønsted acid site while tacking off another H atom to form the Mo−C_6H_{11} intermediate, with a rate-limiting barrier of 1.56 eV, which is 0.25 eV larger than that of ethylene aromatization (1.31 eV). It is revealed that the aromatization process of ethylene intermediate is energetically more advantageous than that of propylene. The calculation results show that the process of methane−methanol coupling to light olefins (mainly ethylene and propylene) is determined by the C−C coupling step, while the further aromatization of ethylene and propylene intermediate is kinetically controlled by the dehydrogenation step to regenerate the Brønsted acid site over Mo/ZSM-5. The in-depth understanding of reaction pathways and kinetic determining steps of methane−methanol coupling reactions over Mo/ZSM-5 is of great assistance to optimize the catalytic activity and tune the selectivity of target product through catalyst modification.

5. Effect of H_2O in Methane−Methanol Coupling Reaction over Mo/ZSM-5. The influence of H_2O on methane−methanol coupling to ethylene and ethylene aromatization to benzene over Mo/ZSM-5 was further investigated since the activation of methanol produces the H_2O molecule. Our previous study on the effect of H_2O on C−C coupling and dehydrogenation reactions involved in methane−methanol coupling to ethylene over Zn/ZSM-5 catalyst showed that the presence of H_2O has little effect on the ethylene formation and the rate-limiting step remains the same as that in the absence of H_2O.[49] In this work, due to the complexity of reaction network for the MDA reaction with methanol over Mo/ZSM-5, we only focused on examining the rate-limiting steps (Mo−CH_3 + O_{fra}−CH_3 → C_2H_6 and cyclo-Mo−C_6H_{11} → Mo−C_6H_{10} + $O_{1\text{-}fra}$−H) with H_2O co-

https://doi.org/10.1021/cbe.3c00021
Chem Bio Eng. 2024, 1, 231−244

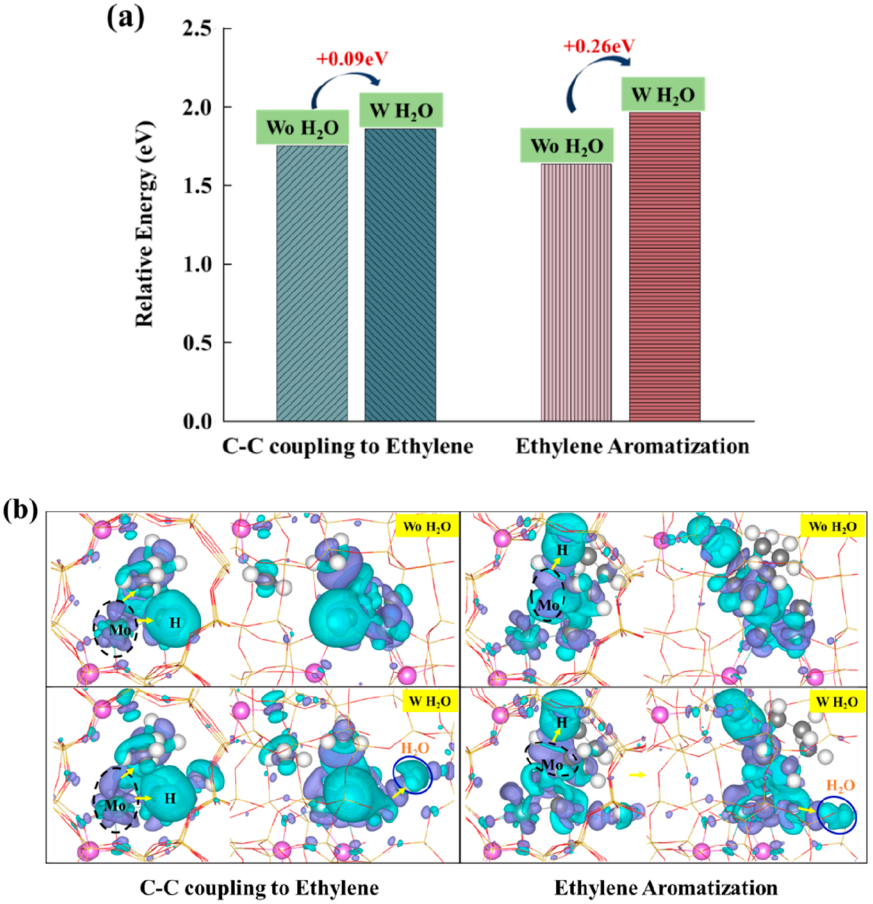

Figure 8. (a) Rate-limiting barriers and (b) differential charge density maps of the transition states for C−C coupling to ethylene and ethylene aromatization to benzene with and without H_2O co-adsorption over Mo/ZSM-5.

adsorption to assess the impact of H_2O on the reactivity. We found that the co-adsorption of H_2O on the Mo site of Mo/ZSM-5 (Figure S7) is 0.57 eV more stable than co-adsorption near the C site of Mo/ZSM-5 (Figure S8). Figure 8(a) shows the comparison of rate-limiting barriers for C−C coupling to ethylene and ethylene aromatization to benzene with and without H_2O co-adsorption over Mo/ZSM-5. The optimized structures of initial, transition, and final states involved in the presence of H_2O co-adsorption are shown in Figure S7. The calculation results show that the rate-limiting barrier (1.49 eV) of methane−methanol coupling to ethylene with H_2O co-adsorption is only 0.09 eV higher than that (1.40 eV) in the absence of H_2O co-adsorption over Mo/ZSM-5. With regard to ethylene aromatization to benzene in the presence of H_2O co-adsorption, the rate-limiting barrier is increased to 1.57 eV, which is 0.26 eV larger than that of ethylene aromatization without H_2O co-adsorption over Mo/ZSM-5. These results indicate that the co-adsorption of H_2O over Mo/ZSM-5 has little influence on the process of C−C coupling forming ethylene, whereas it negatively impacts the rate-limiting step of ethylene aromatization to benzene.

The differential charge density can describe the charge density change around atoms participating in the reaction and help us understand the charge transfer feature in the local reaction area at the atomic level. To gain a deeper understanding of the methane−methanol coupling mechanism and the effect of H_2O co-adsorption, the differential charge density profiles of transition states for C−C coupling to ethylene and ethylene aromatization to benzene with and without H_2O co-adsorption over Mo/ZSM-5 are plotted and shown in Figure 8(b). In the absence of H_2O, it can be seen that the charge mainly transfers from the Mo atom of the Mo Lewis acid site to the C−H species not participating in the reaction, but a small amount of charge transfers to the Mo−CH_3 and O_{fra}−CH_3 species for the C−C coupling reaction in the transition state structure. By contrast, in the presence of H_2O co-adsorption, a portion of charge transfers from the Mo Lewis acid site to the adsorbed H_2O molecule. In the transition state structure of ethylene aromatization to benzene without H_2O co-adsorption, the charge mainly transfers from the Mo atom of the Mo Lewis acid site to the H atom participating in the dehydrogenation reaction (adsorbed to the framework oxygen atom), whereas when H_2O is co-adsorbed over Mo/ZSM-5, there is also a part of charge transfers from Mo Lewis acid site to the adsorbed H_2O. The process of methane−methanol coupling to ethylene is kinetically limited by the C−C coupling of Mo−CH_3 and O_{fra}−CH_3, but the charge transfer property affected by co-adsorbed H_2O is mainly from the Mo Lewis acid site to C−H species that is not directly participating in the reaction; thus, the effect of co-adsorbed H_2O on the rate-limiting barrier of C−C coupling to ethylene is minor (0.09 eV). By contrast, the rate-limiting step of ethylene aromatization is cyclo-Mo−C_6H_{11} dehydrogenation to framework oxygen atom, with a large part of charge transferred from the Mo Lewis acid site to the stripped H. When a H_2O molecule is co-adsorbed, a part of the charge transfers from the

https://doi.org/10.1021/cbe.3c00021
Chem Bio Eng. 2024, 1, 231−244

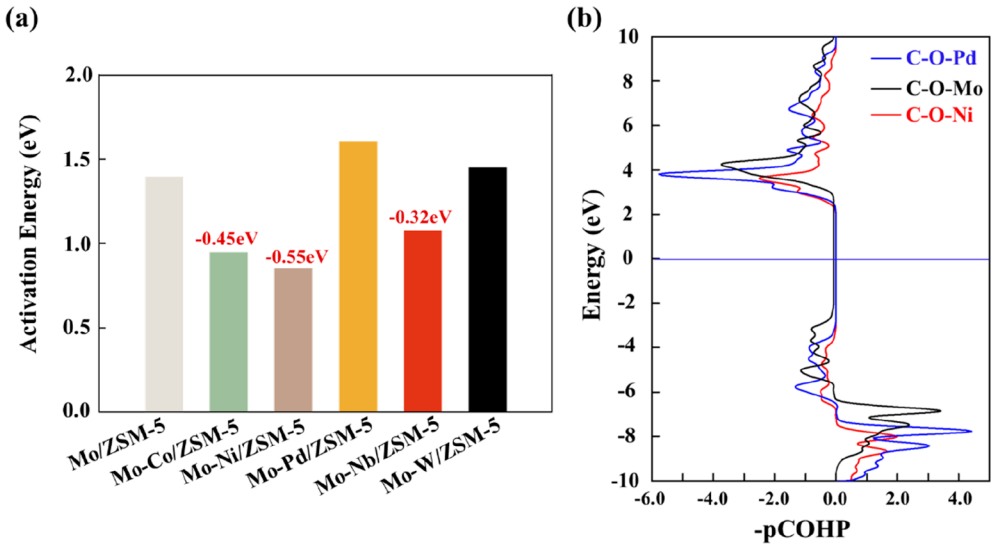

Figure 9. (a) Comparison of rate-limiting barriers for methane−methanol conversion over Mo/ZSM-5 and bimetallic Mo−M/ZSM-5 (M = Co, Ni, Pd, Nb, W) and (b) COHP analysis for the interaction of C−O_{fra} bonds in the reactant state for the rate-limiting C−C coupling step over Mo/ZSM-5, Mo−Ni/ZSM-5, and Mo−Pd/ZSM-5.

Mo Lewis acid site to the H of the H_2O molecule, thus directly affecting the dehydrogenation property and leading to an increased rate-limiting barrier (0.26 eV) of ethylene aromatization to benzene over Mo/ZSM-5. These calculation results provide important insight into understanding the effect of H_2O on C−C coupling and ethylene aromatization over Mo/ZSM-5 according to reaction energetics calculations and charge transfer property analysis, as discussed above.

6. Screening for Promising Bimetallic Mo−M/ZSM-5 Catalysts for Methane Nonoxidative Conversion. Although the Mo species is one of the active components for methane nonoxidative conversion, the activity and stability of Mo/zeolite catalysts still need to be improved due to the detrimental coke formation that causes relatively fast deactivation of the catalyst. According to previous studies on methane dehydrogenation and aromatization over Mo/ZSM-5, introducing a second metal component such as Nb, Co, or W into Mo/ZSM-5 has potential advantages in regulating the electronic feature of Mo and stabilizing the Mo active sites.[50−56] The above calculation results show that the processes of C−C coupling to ethylene followed by ethylene aromatization are kinetically more favorable than those via the propylene intermediate in the methane−methanol coupling reaction. Thus, the bimetallic screening study was focused on the rate-limiting steps involved in ethylene formation and its aromatization. The energy diagrams plotted in Figure 3(a) and Figure 5 show that the elementary step of Mo−CH_3 and O_{fra}−CH_3 direct coupling determines the overall rate for methane−methanol conversion to benzene over Mo/ZSM-5 catalyst due to the highest barrier of 1.40 eV. Herein, we examined the addition of second modification components to further regulate the catalytic activity of Mo/ZSM-5 for methane−methanol coupling reaction. Co, Ni, Pd, Nb, and W were preliminarily selected as the second modifiers for Mo/ZSM-5, by replacing a Mo atom in the $[Mo_4C_2]^{2+}$ species with each of the metals (denoted as Mo−M/ZSM-5). The rate-limiting C−C coupling step (Mo−CH_3 + O_{fra}−CH_3 → C_2H_6) identified over Mo/ZSM-5 was used as the screening descriptor for these bimetallic Mo−M/ZSM-5 candidates.

The activation barrier and Crystal Orbital Hamilton Population (COHP) analysis of the rate-limiting step (M−CH_3 + O_{fra}−CH_3 → C_2H_6) for methane−methanol conversion over Mo/ZMS-5 and bimetallic Mo−M/ZSM-5 catalysts are shown in Figure 9, while the optimized structures involved are provided in Figure S9. As shown in Figure 9(a), the C−C coupling barriers over Mo−Co/ZSM-5, Mo−Ni/ZSM-5, and Mo−Nb/ZSM-5 are 0.95, 0.85, and 1.08 eV, respectively, which are 0.32−0.55 eV smaller than that (1.40 eV) obtained over Mo/ZSM-5. However, the C−C coupling barrier on Mo−Pd/ZSM-5 is 1.60 eV, which is larger than that over Mo/ZSM-5. The addition of W into Mo/ZSM-5 has little effect on the C−C coupling reaction with a barrier of 1.45 eV. The COHP analysis was further utilized to analyze the effect of adding a second metal component into Mo/ZSM-5 on the methane−methanol coupling reaction to understand the chemical bond interactions of the studied system. Based on the comparison of rate-limiting barriers as shown in Figure 9(a), the bimetallic Mo−Ni/ZSM-5 is proposed as the most promising candidate for methane−methanol coupling due to the lowest rate-limiting barrier (0.85 eV), whereas the bimetallic Mo−Pd/ZSM-5 is obviously less active than Mo/ZSM-5. Therefore, the C−O interactions of the O_{fra}−CH_3 species in the reactant state structures for the rate-limiting C−C coupling step over Mo−Ni/ZSM-5, Mo/ZSM-5, and Mo−Pd/ZSM-5 were further analyzed by the COHP calculation, and the results are shown in Figure 9(b). The calculated integral values below the Fermi level for C−O interactions are −4.28, −6.06, and −8.54 eV, respectively, in the O_{fra}−CH_3 species over Mo−Ni/ZSM-5, Mo/ZSM-5, and Mo−Pd/ZSM-5. The larger the absolute integral value, the stronger the chemical bonding interaction; hence the C−O bonding strength in the reactant state structure is in the sequence Mo−Ni/ZSM-5 < Mo/ZSM-5 < Mo−Pd/ZSM-5. Therefore, the C−C coupling barrier contributed from the C−O bond breaking in the O_{fra}−CH_3 species should be smaller over Mo−Ni/ZSM-5 than that on Mo/ZSM-5, while introducing Pd increases the C−C coupling barrier due to the stronger C−O bonding interaction in the O_{fra}−CH_3 species over Mo−Pd/ZSM-5. The calculation results from COHP analysis are consistent with the barrier

https://doi.org/10.1021/cbe.3c00021
Chem Bio Eng. 2024, 1, 231−244

calculation trend. The computational screening results reveal that the bimetallic Mo−Co/ZSM-5, Mo−Ni/ZSM-5, and Mo−Nb/ZSM-5 are promising candidates for methane−methanol coupling reaction, with Mo−Ni/ZSM-5 as the most outstanding contender. This computational work provides useful guidance for future design of efficient metal/zeolite catalysts for the methane−methanol coupling reaction.

CONCLUSIONS

In this work, the reaction pathways and energy profiles of the methane−methanol coupling reaction over Mo/ZSM-5 are studied by periodic DFT calculations. The reaction intermediates, transition states, and optimal reaction routes of methane−methanol coupling to light olefins (ethylene and propylene) and their further aromatization to benzene over Mo/ZSM-5 are identified. The rate-limiting step for methane−methanol coupling to ethylene is the coupling of Mo−CH_3 and O_{fra}−CH_3 species, while that for propylene formation is the Mo−CH_3 directly coupling with ethylene, with rate-limiting barriers of 1.40 and 1.43 eV, respectively. Unlike the processes of C−C coupling to ethylene and propylene, the rate-limiting steps of ethylene and propylene aromatization to benzene are both involved in the dehydrogenation processes to regenerate the Brønsted acid site, with rate-limiting barriers of 1.31 and 1.56 eV, respectively. The calculation results indicate that the process of methane−methanol coupling to light olefins is determined by the C−C coupling reactions, while the further aromatization is mainly controlled by the dehydrogenation reactions for regeneration of the Brønsted acid site over Mo/ZSM-5. The overall reaction shows that the methane−methanol coupling to aromatic products proceeds more favorably with ethylene as the intermediate product than propylene. In addition, it is found that the co-adsorption of H_2O nearby has little effect on methane−methanol coupling to ethylene, whereas it causes an increase of the rate-limiting barrier (by 0.26 eV) for ethylene aromatization to benzene. The introduction of Co, Ni, or Nb as a second modification component into Mo/ZSM-5 can reduce the rate-limiting C−C coupling barrier by 0.32−0.55 eV in the methane−methanol coupling reaction, with bimetallic Mo−Ni/ZSM-5 as the most promising candidate.

ASSOCIATED CONTENT

Supporting Information

The Supporting Information is available free of charge at https://pubs.acs.org/doi/10.1021/cbe.3c00021.

Optimized structures of catalyst models and all states involved in different reaction steps. (PDF)

AUTHOR INFORMATION

Corresponding Authors

Xiaowa Nie − *State Key Laboratory of Fine Chemicals, Frontier Science Center for Smart Materials, PSU-DUT Joint Center for Energy Research, School of Chemical Engineering, Dalian University of Technology, Dalian 116024, China;* orcid.org/0000-0002-9937-5456; Email: niexiaowa@dlut.edu.cn

Chunshan Song − *State Key Laboratory of Fine Chemicals, Frontier Science Center for Smart Materials, PSU-DUT Joint Center for Energy Research, School of Chemical Engineering, Dalian University of Technology, Dalian 116024, China; Department of Chemistry, Faculty of Science, The Chinese University of Hong Kong, Shatin, NT 999077, China;* orcid.org/0000-0003-2344-9911; Email: chunshansong@cuhk.edu.hk

Xinwen Guo − *State Key Laboratory of Fine Chemicals, Frontier Science Center for Smart Materials, PSU-DUT Joint Center for Energy Research, School of Chemical Engineering, Dalian University of Technology, Dalian 116024, China;* orcid.org/0000-0002-6597-4979; Email: guoxw@dlut.edu.cn

Authors

Mengnan Sun − *State Key Laboratory of Fine Chemicals, Frontier Science Center for Smart Materials, PSU-DUT Joint Center for Energy Research, School of Chemical Engineering, Dalian University of Technology, Dalian 116024, China*

Xinwei Zhang − *Dalian Research Institute of Petroleum and Petrochemicals, SINOPEC, Dalian 116041, China*

Sirui Liu − *State Key Laboratory of Fine Chemicals, Frontier Science Center for Smart Materials, PSU-DUT Joint Center for Energy Research, School of Chemical Engineering, Dalian University of Technology, Dalian 116024, China*

Complete contact information is available at: https://pubs.acs.org/10.1021/cbe.3c00021

Author Contributions

#M.S. and X.N. contributed equally to this work.

Notes

The authors declare no competing financial interest.

ACKNOWLEDGMENTS

This work is supported by the Natural Science Foundation of Liaoning Province (No. 2023-MS-105), the Fundamental Research Funds for the Central Universities (No. DUT22-LAB602), and Liaoning Revitalization Talents Program (No. XLYC2008032). We acknowledge the Supercomputing Center of Dalian University of Technology and Tianjin Supercomputing Center for providing computing resources for this work.

REFERENCES

(1) Xu, Y.; Bao, X.; Lin, L. Direct conversion of methane under nonoxidative conditions. *Journal of Catalysis* **2003**, *216* (1-2), 386−395.

(2) Zheng, H.; Ma, D.; Liu, X.; Zhang, W.; Han, X.; Xu, Y.; Bao, X. Methane dehydroaromatization over Mo/HZSM-5: A study of catalytic process. *Catalysis Letters* **2006**, *111* (1-2), 111−114.

(3) Karakaya, C.; Morejudo, S. H.; Zhu, H.; Kee, R. J. Catalytic Chemistry for Methane Dehydroaromatization (MDA) on a Bifunctional Mo/HZSM-5 Catalyst in a Packed Bed. *Industrial & Engineering Chemistry Research* **2016**, *55* (37), 9895−9906.

(4) Kosinov, N.; Coumans, F. J. A. G.; Li, G.; Uslamin, E.; Mezari, B.; Wijpkema, A. S. G.; Pidko, E. A.; Hensen, E. J. M. Stable Mo/HZSM-5 methane dehydroaromatization catalysts optimized for high-temperature calcination-regeneration. *Journal of Catalysis* **2017**, *346*, 125−133.

(5) Liu, H.; Shen, W.; Bao, X.; Xu, Y. Identification of Mo active species for methane dehydro-aromatization over Mo/HZSM-5 catalysts in the absence of oxygen: 1H MAS NMR and EPR investigations. *J. Mol. Catal. A: Chem.* **2006**, *244* (1-2), 229−236.

(6) Wang, L. S.; Tao, L. X.; Xie, M. S.; Xu, G. F.; Huang, J. S.; Xu, Y. D. DEHYDROGENATION AND AROMATIZATION OF METHANE UNDER NONOXIDIZING CONDITIONS. *Catalysis Letters* **1993**, *21* (1-2), 35−41.

(7) Ismagilov, Z. R.; Matus, E. V.; Tsikoza, L. T. Direct conversion of methane on Mo/ZSM-5 catalysts to produce benzene and

hydrogen: achievements and perspectives. *Energy Environ. Sci.* **2008**, *1* (5), 526.
(8) Ma, S.; Guo, X.; Zhao, L.; Scott, S.; Bao, X. Recent progress in methane dehydroaromatization: From laboratory curiosities to promising technology. *Journal of Energy Chemistry* **2013**, *22* (1), 1−20.
(9) Tempelman, C. H. L.; Hensen, E. J. M. On the deactivation of Mo/HZSM-5 in the methane dehydroaromatization reaction. *Applied Catalysis B: Environmental* **2015**, *176-177*, 731−739.
(10) Wong, K. S.; Thybaut, J. W.; Tangstad, E.; Stöcker, M. W.; Marin, G. B. Methane aromatisation based upon elementary steps: Kinetic and catalyst descriptors. *Microporous and Mesoporous Materials* **2012**, *164*, 302−312.
(11) Tan, P. Ammonia-basified 10 wt% Mo/HZSM-5 material with enhanced dispersion of Mo and performance for catalytic aromatization of methane. *Applied Catalysis A: General* **2019**, *580*, 111−120.
(12) Danhong; Zhou; Ding; Ma; Xianchun; Liu; Xinhe. A simulation study on the absorption of molybdenum species in the channels of HZSM-5 zeolite. *Journal of Molecular Catalysis A Chemical* **2001**, *168*, 225.
(13) Li, W.; Meitzner, G. D.; Borry, R. W.; Iglesia, E. Raman and X-Ray Absorption Studies of Mo Species in Mo/H-ZSM5 Catalysts for Non-Oxidative CH_4 Reactions. *Journal of Catalysis* **2000**, *191* (2), 373−383.
(14) Tessonnier, J.-P.; Louis, B.; Rigolet, S.; Ledoux, M. J.; Pham-Huu, C. Methane dehydro-aromatization on Mo/ZSM-5: About the hidden role of Brønsted acid sites. *Applied Catalysis A: General* **2008**, *336* (1-2), 79−88.
(15) Tessonnier, J. P.; Louis, B.; Walspurger, S.; Sommer, J.; Ledoux, M. J.; Pham-Huu, C. Quantitative Measurement of the Brönsted Acid Sites in Solid Acids: Toward a Single-Site Design of Mo-Modified ZSM-5 Zeolite. *J. Phys. Chem. B* **2006**, *110*, 10390−10395.
(16) Zheng, H.; Ma, D.; Bao, X.; Hu, J. Z.; Kwak, J. H.; Wang, Y.; Peden, C. H. F. Direct observation of the active center for methane dehydroaromatization using an ultrahigh field 95Mo NMR spectroscopy. *J. Am. Chem. Soc.* **2008**, *130* (12), 3722−3.
(17) Zhou, D.; Ma, D.; Liu, X.; Bao, X. Study with density functional theory method on methane dehydro-aromatization over Mo/HZSM-5 catalysts I: Optimization of active Mo species bonded to ZSM-5 zeolite. *J. Chem. Phys.* **2001**, *114* (20), 9125−9129.
(18) Kim, Y.-H.; Borry, R. W; Iglesia, E. Genesis of methane activation sites in Mo-exchanged H-ZSM-5 catalysts. *Microporous and Mesoporous Materials* **2000**, *35-36* (none), 495−509.
(19) Lezcano-Gonzalez, I.; Oord, R.; Rovezzi, M.; Glatzel, P.; Botchway, S. W.; Weckhuysen, B. M.; Beale, A. M. Molybdenum Speciation and its Impact on Catalytic Activity during Methane Dehydroaromatization in Zeolite ZSM-5 as Revealed by Operando X-Ray Methods. *Angew. Chem. Int. Ed Engl* **2016**, *55* (17), 5215−9.
(20) Gao, J.; Zheng, Y.; Jehng, J.-M.; Tang, Y.; Wachs, I. E.; Podkolzin, S. G. Identification of molybdenum oxide nanostructures on zeolites for natural gas conversion. *Science* **2015**, *348*, 686.
(21) Rahman, M.; Infantes-Molina, A.; Hoffman, A. S.; Bare, S. R.; Emerson, K. L.; Khatib, S. J. Effect of Si/Al ratio of ZSM-5 support on structure and activity of Mo species in methane dehydroaromatization. *Fuel* **2020**, *278*, 118290.
(22) Wang, D.; Lunsford, J. H.; Rosynek, M. P. Characterization of a Mo/ZSM-5 Catalyst for the Conversion of Methane to Benzene. *Journal of Catalysis* **1997**, *169* (1), 347−358.
(23) Wang, D.; Lunsford, J. H.; Rosynek, M. P. Catalytic conversion of methane to benzene over Mo/ZSM-5. *Top. Catal.* **1996**, *3* (3), 289−297.
(24) Konnov, S. V.; Dubray, F.; Clatworthy, E. B.; Kouvatas, C.; Gilson, J. P.; Dath, J. P.; Minoux, D.; Aquino, C.; Valtchev, V.; Moldovan, S.; Koneti, S.; Nesterenko, N.; Mintova, S. Novel Strategy for the Synthesis of Ultra-Stable Single-Site Mo-ZSM-5 Zeolite Nanocrystals. *Angewandte Chemie* **2020**, *59* (44), 19553−19560.
(25) Xi, Z.; Zhou, B.; Yu, Y.; Jiang, B.; Liao, Z.; Wang, J.; Huang, Z.; Yang, Y.; Sun, J.; Yang, Y. Enhancing low-temperature methane conversion on Zn/ZSM-5 in the presence of methanol by regulating the methanol-to-aromatics reaction pathway. *Catalysis Science & Technology* **2020**, *10* (18), 6161−6172.
(26) Majhi, S.; Dalai, A. K.; Pant, K. K. Methanol assisted methane conversion for higher hydrocarbon over bifunctional Zn-modified Mo/HZSM-5 catalyst. *J. Mol. Catal. A: Chem.* **2015**, *398*, 368−375.
(27) Majhi, S.; Pant, K. K. Direct conversion of methane with methanol toward higher hydrocarbon over Ga modified Mo/H-ZSM-5 catalyst. *Journal of Industrial and Engineering Chemistry* **2014**, *20* (4), 2364−2369.
(28) Choudhary, V. R.; Mondal, K. C.; Mulla, S. A. Simultaneous conversion of methane and methanol into gasoline over bifunctional Ga-, Zn-, In-, and/or Mo-modified ZSM-5 zeolites. *Angewandte Chemie* **2005**, *44* (28), 4381−5.
(29) Liu, Y.; Li, D.; Wang, T.; Liu, Y.; Xu, T.; Zhang, Y. Efficient Conversion of Methane to Aromatics by Coupling Methylation Reaction. *ACS Catal.* **2016**, *6* (8), 5366−5370.
(30) Liu, S.; Bian, K.; Yang, H.; Sun, M.; Nie, X.; Zhang, X.; Hou, S.; Zhang, G.; Song, C.; Guo, X. Methane transformation into light olefins using methanol as co-reactant over Mo/HZSM-5. *Chemical Engineering Science* **2024**, *283*, 119431.
(31) Baerlocher, C.; Mccusker, L. B. J. M.; Materials, M. Database of Zeolite Structures. *Microporous and Mesoporous Materials* **2020**, *297*, 110000.
(32) Yin, F.; Li, M. R.; Wang, G. C. Periodic density functional theory analysis of direct methane conversion into ethylene and aromatic hydrocarbons catalyzed by Mo(4)C(2)/ZSM-5. *Phys. Chem. Chem. Phys.* **2017**, *19* (33), 22243−22255.
(33) Shetty, S.; Sivakumar, S.; Jana, S. K.; Sreenivasarao, G. Investigation of CHx (x = 2-4) Adsorption on Mo2C and Mo4C2 Sites Incorporated in ZSM-5 Zeolite Using Periodic-DFT Approach. *Catalysis Letters* **2018**, *148* (1), 68−78.
(34) Kresse, G.; Furthmüller, J. Efficiency of ab-initio total energy calculations for metals and semiconductors using a plane-wave basis set. *Computational Materials Science* **1996**, *6* (1), 15−50.
(35) Kresse, G.; Joubert, D. From ultrasoft pseudopotentials to the projector augmented-wave method. *Phys. Rev. B* **1999**, *59* (3), 1758−1775.
(36) Blöchl, P. E. Projector augmented-wave method. *Phys. Rev. B* **1994**, *50*, 17953−17979.
(37) Perdew, J. P.; Burke, K.; Ernzerhof, M. Generalized gradient approximation made simple. *Physical Review Letters* **1996**, *77* (18), 3865−3868.
(38) Grimme, S. Accurate description of van der Waals complexes by density functional theory including empirical corrections. *Journal of Computational Chemistry* **2004**, *25* (12), 1463−1473.
(39) Grimme, S.; Antony, J.; Schwabe, T.; Mück-Lichtenfeld, C. Density functional theory with dispersion corrections for supramolecular structures, aggregates, and complexes of (bio)organic molecules. *Organic & Biomolecular Chemistry* **2007**, *5* (5), 741−758.
(40) Henkelman, G.; Uberuaga, B. P.; Jonsson, H. A climbing image nudged elastic band method for finding saddle points and minimum energy paths. *J. Chem. Phys.* **2000**, *113* (22), 9901−9904.
(41) Kosinov, N.; Hensen, E. J. M. Reactivity, Selectivity, and Stability of Zeolite-Based Catalysts for Methane Dehydroaromatization. *Adv. Mater.* **2020**, *32* (44), No. e2002565.
(42) Gomez, E.; Nie, X.; Lee, J. H.; Xie, Z.; Chen, J. G. Tandem Reactions of CO(2) Reduction and Ethane Aromatization. *J. Am. Chem. Soc.* **2019**, *141* (44), 17771−17782.
(43) Li, D.; Xing, B.; Wang, B.; Li, R. Activity and selectivity of methanol-to-olefin conversion over Zr-modified H-SAPO-34/H-ZSM-5 zeolites - A theoretical study. *Fuel Processing Technology* **2020**, *199*, 106302.
(44) Tu, C.; Fan, H.; Wang, D.; Rui, N.; Du, Y.; Senanayake, S. D.; Xie, Z.; Nie, X.; Chen, J. G. CO2-assisted ethane aromatization over zinc and phosphorous modified ZSM-5 catalysts. *Applied Catalysis B: Environmental* **2022**, *304*, 120956.
(45) Wang, S.; Li, S.; Zhang, L.; Qin, Z.; Chen, Y.; Dong, M.; Li, J.; Fan, W.; Wang, J. Mechanistic insights into the catalytic role of various acid sites on ZSM-5 zeolite in the carbonylation of methanol

https://doi.org/10.1021/cbe.3c00021
Chem Bio Eng. 2024, 1, 231−244

and dimethyl ether. *Catalysis Science & Technology* **2018**, *8* (12), 3193−3204.
(46) Yin, F.; Li, M. R.; Wang, G. C. Periodic density functional theory analysis of direct methane conversion into ethylene and aromatic hydrocarbons catalyzed by Mo_4C_2/ZSM-5. *Phys. Chem. Chem. Phys.* **2017**, *19* (33), 22243−22255.
(47) Biscardi, J. A.; Iglesia, E. Reaction Pathways and Rate-Determining Steps in Reactions of Alkanes on H-ZSM5 and Zn/H-ZSM5 Catalysts. *Journal of Catalysis* **1999**, *182* (1), 117−128.
(48) Biscardi, J. A.; Iglesia, E. Non-oxidative reactions of propane on Zn/Na-ZSM5. *Physical Chemistry Chemical Physics* **1999**, *1* (24), 5753−5759.
(49) Sun, M.; Nie, X.; Zhang, X.; Liu, S.; Song, C.; Guo, X. Computational identification of bifunctional metal-modified ZSM-5 catalysts to boost methane-methanol coupling. *Catalysis Science & Technology* **2022**, *12* (24), 7328−7340.
(50) Cheng, J.; Huang, W. Effect of cobalt (nickel) content on the catalytic performance of molybdenum carbides in dry-methane reforming. *Fuel Processing Technology* **2010**, *91* (2), 185−193.
(51) Du, X.; Liu, J.; Li, D.; Xin, H.; Lei, X.; Zhang, R.; Zhou, L.; Yang, H.; Zeng, Y.; Zhang, H.; Zheng, W.; Wen, X.; Hu, C. Structural and electronic effects boosting Ni-doped Mo2C catalyst toward high-efficiency CO/CC bonds cleavage. *Journal of Energy Chemistry* **2022**, 75, 109−116.
(52) Jiménez, M. J.; Lissarrague, M. S.; Bechthold, P.; González, E. A.; Jasen, P. V.; Juan, A. Ethanol adsorption on Ni doped $Mo_2C(001)$: a theoretical study. *Top. Catal.* **2022**, *65* (7-8), 839−847.
(53) Liu, J.; Hodes, G.; Yan, J.; Liu, S. Metal-doped Mo2C (metal = Fe, Co, Ni, Cu) as catalysts on TiO2 for photocatalytic hydrogen evolution in neutral solution. *Chinese Journal of Catalysis* **2021**, *42* (1), 205−216.
(54) Pasupulety, N.; Al-Zahrani, A. A.; Daous, M. A.; Driss, H.; Petrov, L. A. Methane aromatization study on M-Mo2C/HZSM-5 (M = Ce or Pd or Nb) nano materials. *Journal of Materials Research and Technology* **2021**, *14*, 363−373.
(55) Sridhar, A.; Rahman, M.; Infantes-Molina, A.; Wylie, B. J.; Borcik, C. G.; Khatib, S. J. Bimetallic Mo-Co/ZSM-5 and Mo-Ni/ZSM-5 catalysts for methane dehydroaromatization: A study of the effect of pretreatment and metal loadings on the catalytic behavior. *Applied Catalysis A: General* **2020**, *589*, 117247.
(56) Wang, F.; Li, T.; Shi, Y.; Jiao, H. Molybdenum carbide supported metal catalysts (Mn/MoxC; M = Co, Ni, Cu, Pd, Pt) - metal and surface dependent structure and stability. *Catalysis Science & Technology* **2020**, *10* (9), 3029−3046.

https://doi.org/10.1021/cbe.3c00021
Chem Bio Eng. 2024, 1, 231−244